

pubs.acs.org/acsapm Article

# Mechanically Induced Elastomeric Optical Transmittance Modulator

Fangqi Chen, Yanpei Tian, Xiaojie Liu, Andrew Caratenuto, and Yi Zheng\*



**Cite This:** ACS Appl. Polym. Mater. 2021, 3, 5434–5440



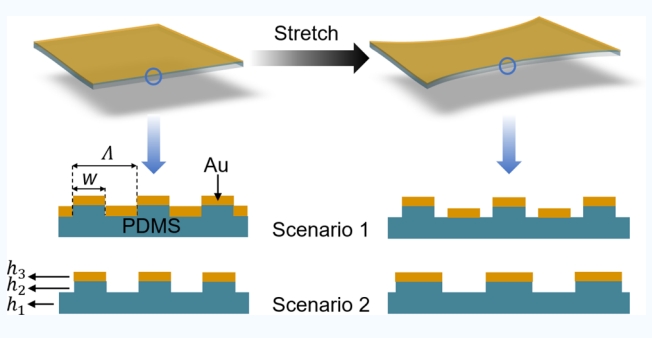
**ACCESS** 

Metrics & More



SI Supporting Information

ABSTRACT: Optical devices with switchable optical properties have attracted great interest in recent years because of their extensive engineering applications. The dynamic tuning of optical properties can be triggered by various types of external stimuli. In this work, a mechanically induced elastomeric optical transmittance modulator is reported. The design is composed of poly-(dimethylsiloxane), a silicone-based rubber transparent at visible wavelengths, with gold nanofilms deposited on the surface. The influence of geometric parameters on the total transmittance is studied utilizing the Rigorous Coupled Wave Analysis model. Taking advantage of the excellent stretching capacity of the



elastomer, reversible modulation of both normal and total transmittance is achieved. A 42% rise in the total transmittance is realized under a strain of 80%. Cycle testing illustrates stable structural integrity and optical performance even after repeated strain cycles. This elastomeric optical transmittance modulator opens avenues for practical applications due to its simple design and facile tunability.

KEYWORDS: optical modulator, elastomer, mechanically induced, tunable optical transmittance, smart windows

#### ■ INTRODUCTION

The dynamic tuning of optical transmittance has recently attracted significant attention due to various promising applications, such as smart windows, <sup>1–5</sup> sensing devices, <sup>6</sup> and optical data storage. <sup>7,8</sup> Many strategies and materials have been introduced to realize switchable optical properties. Notable techniques include suspended particles, <sup>9</sup> liquid crystals, <sup>10</sup> and chromogenic materials designed to respond to external optical, <sup>11,12</sup> thermal, <sup>13</sup> electrical, <sup>5,14,15</sup> and chemical stimuli. <sup>16</sup> However, barriers to practical applications still persist, such as complicated fabrication processes and chemical instability. <sup>17</sup> Among the aforementioned external stimuli which are used to tune optical properties, reversible tuning by mechanical forces is the most straightforward method and possesses the merit of a rapid responsive time, thus drawing a great deal of attention. <sup>18,19</sup>

Polymer science has been designated as "the gateway to the future," as it deals with our capability to develop ever-more sophisticated materials to suit the desires of society and the planet. Deliver are serving a vital role in various state-of-the-art sustainable energy technologies such as triboelectric nanogenerators, Supercapacitor, And piezoelectric generator. Poly(dimethylsiloxane) (PDMS), an optically transparent elastomer, is commonly used for engineering applications such as smart windows due to its transparency over solar wavelengths and mechanical properties favorable for stretching. Many elastomer-based devices have been proposed in recent years, which utilize various dynamic tuning strategies, including mechanically controlled voids, surface-texturing

with nanopillars, <sup>29,30</sup> magnetically tunable structures, <sup>31</sup> embedded silica nanoparticles,1 crumpling of metallic nanofilms, graphene films, and graphene oxide films.<sup>32–34</sup> Jiang et al. proposed a generalized synthesis strategy for fabricating reversible surface wrinkles on elastomeric PDMS substrates with different skin layer materials, such as poly(vinyl alcohol). The bilayer film can be switched between a transparent stretched state and an opaque released state upon moderate stretching.<sup>35</sup> Li et al. reported a highly effective one-step fabrication method by ultraviolet/ozone etching the surface of a freestanding PDMS film. A large transmittance tuning range was realized by harnessing the wrinkling-cracking patterns on the surface.<sup>17</sup> It should be noted that in these studies, the high transmittance change is actually normal transmittance. The surface roughness helps to scatter the incident light rather than block or absorb the light, resulting in a slight total transmittance reduction as a result of an increased strain.

In this paper, a PDMS-based elastomeric grating with nanometer-thick gold (Au) layers deposited on the surface is presented. A SU-8 grating mold is fabricated using photolithography, which is followed by PDMS curing and electron beam evaporation. Two deposition scenarios are fabricated.

Received: June 30, 2021 Accepted: September 16, 2021 Published: September 30, 2021





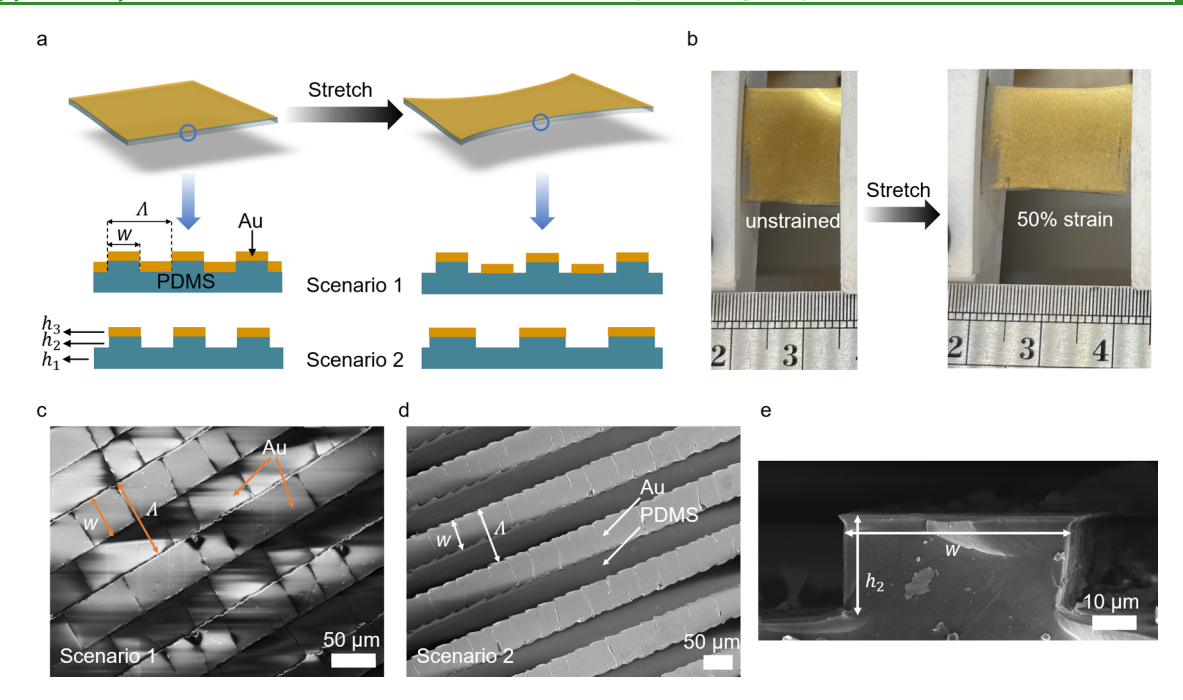


Figure 1. (a) Schematic illustration of the stretching process of the Au-deposited elastomer. Scenario 1: Au deposited on all surfaces of PDMS. Scenario 2: Au only deposited on PDMS gratings. (b) Sample of Scenario 1 stretching from the original, unstrained state to a state with 50% strain. The scanning electron microscopy (SEM) images of (c) a Scenario 1 sample, (d) a Scenario 2 sample, and (e) the cross section view of a Scenario 1 sample.

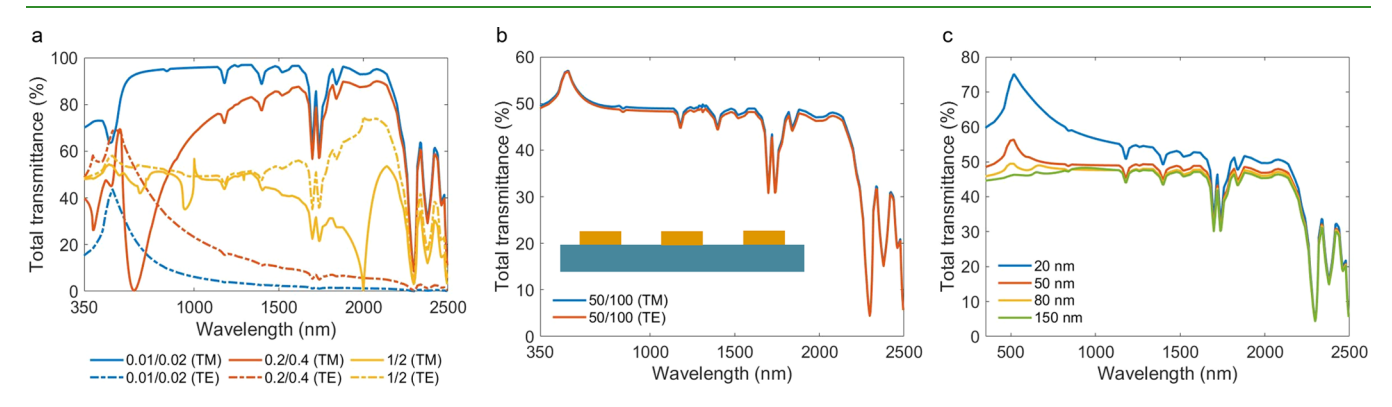


Figure 2. Total transmittance spectra for the grating structure (shown in the inset of (b)) from 350 to 2500 nm, calculated using the RCWA model. (a) Transmittance spectra of three different grating structures. Solid lines show TM polarizations, and dashed lines show TE polarizations. The unit in the legend is  $\mu$ m. (b) Transmittance spectra of the grating structure with  $w/\Lambda = 50/100 \ \mu$ m. (c) Grating structures with varying values of  $h_3$ .

For Scenario 1, Au is present on all of the surfaces of PDMS, shown in Figure 1a, such that the original unstrained state is totally opaque. For Scenario 2, Au is only on the PDMS grating fabricated by the oblique angle deposition method. A geometric parameter study is also conducted using the Rigorous Coupled Wave Analysis (RCWA) model, which considers the width and period of the grating, as well as the thickness of Au layers. For Scenario 1, when subjected to mechanical stress, the average normal optical transmittance can be tuned from 5 to 20%, and the experimental results match well with the calculated RCWA results. The optical tuning range can be further improved when considering the total transmittance instead of just the normal transmittance. Transmittance modulators utilizing surface wrinkles are only able to affect the normal transmittance, as their surface geometries scatter incident light instead of reflecting it. 17 In contrast, Au utilized herein reflects the incident light, allowing for the dynamic tuning of total transmittance and further

expanding the applicability of this technique. Moreover, the Au-deposited elastomer can be reversibly cycled without sacrificing structural integrity or optical performance. This elastomeric optical transmittance modulator sheds light on optical systems that make tunable interactions with light possible and can also be leveraged for potential applications such as smart windows.

## ■ RESULTS AND DISCUSSION

Figure 1a schematically shows the stretching process of the Audeposited elastomer. The width of the grating is represented by w, and  $\Lambda$  is the grating period. PDMS substrate, PDMS grating, and Au thicknesses are, respectively, given by  $h_1$ ,  $h_2$ , and  $h_3$ . Two elastomer fabrication scenarios are introduced: Au deposited on all surfaces of PDMS (Scenario 1) and Au deposited only on the PDMS grating surfaces (Scenario 2). When the Scenario 1 elastomer is subjected to lateral mechanical stress perpendicular to the length of the grating,

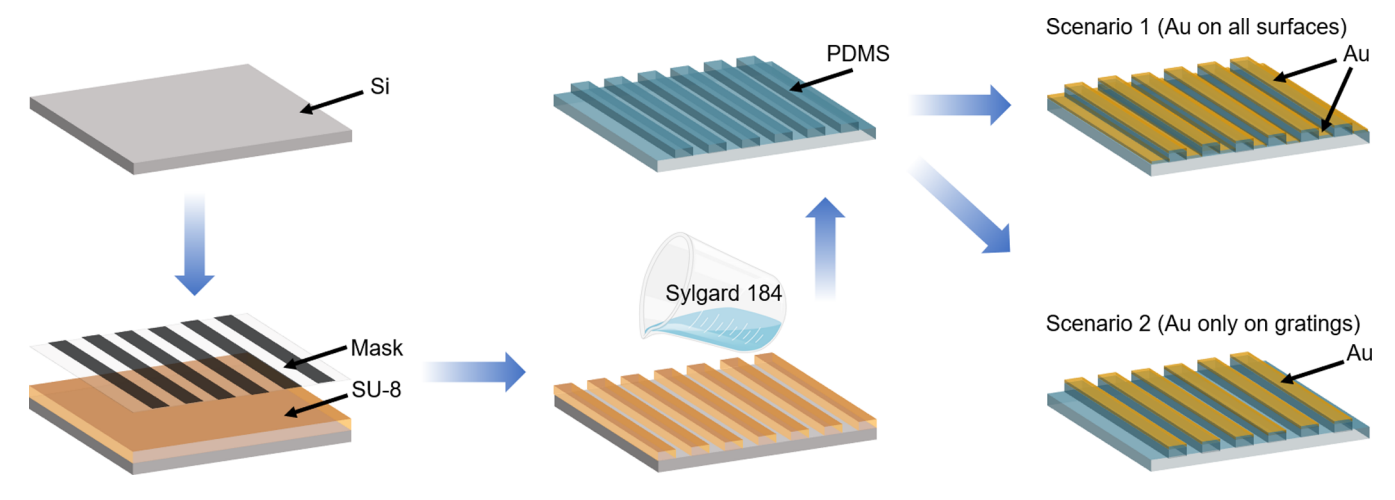


Figure 3. Fabrication process of the Au-deposited elastomer, including photolithography, PDMS curing, and electron beam evaporation. There are two scenarios for fabricated elastomers: Au on all of the surfaces of PDMS (Scenario 1) and Au only on the PDMS gratings (Scenario 2).

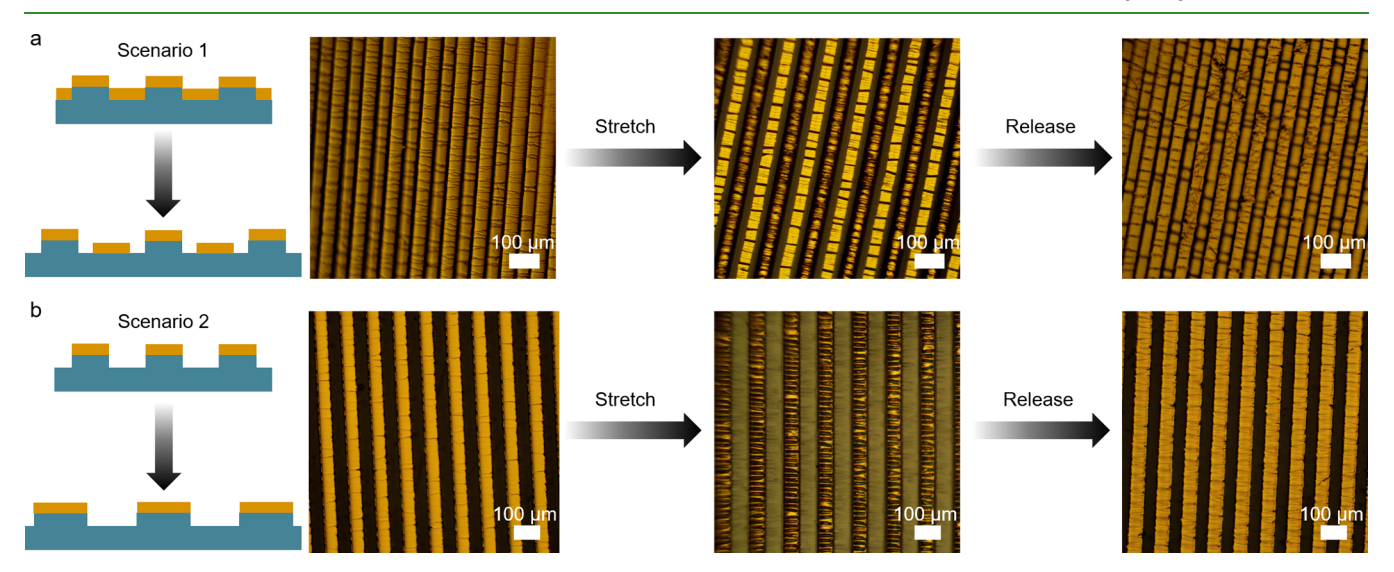


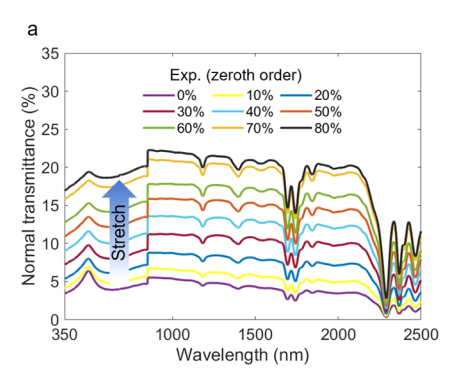
Figure 4. Microscopic images of the Au-deposited elastomer in its original unstrained state, under an applied stress, and after the stress is released.
(a) Scenario 1 and (b) Scenario 2.

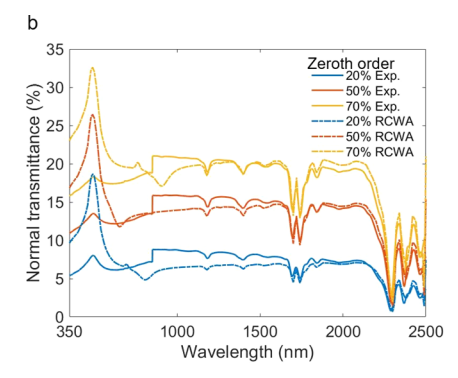
additional PDMS substrate becomes exposed to the incoming light. Two PDMS areas with equivalent widths appear on either side of Au layers between the gratings; thus, modifying the way light interacts with the structure as a whole. In Scenario 2, the widths of gratings and grooves elongate in the same proportion. The precise control of strain is realized by a custom-built stretching device based on a high-precision displacement-sliding table (Figure 1b). The morphology of the elastomer is shown by scanning electron microscopy (SEM) images. Figure 1c,1d provides top views of the corresponding scenarios, in which w and  $\Lambda$  are 50 and 100  $\mu$ m, respectively. Figure 1e presents the cross section of one grating for Scenario 1 with  $h_2$  equals to 25  $\mu$ m.

The geometric parameters of the grating structure are studied using the RCWA model to identify a suitable structure for experimental tests. The thickness of the PDMS grating layer  $h_2$  has little impact on the calculated transmittance because the PDMS substrate layer  $h_1$  is much thicker than  $h_2$ . Therefore, this layer is removed for calculation for the sake of simplicity. Similarly, little attention is paid to variations in the thickness of the PDMS substrate  $h_1$ . This value must be thick enough to maintain a freestanding structure but not too thick

to render stretching difficult. Therefore, a value of  $h_1 = 0.7$  mm is chosen to satisfy both structural stability and elasticity. In the following analyses,  $h_3 = 50$  nm for Figure 2a,b and w = 50 and  $\Lambda = 100 \ \mu m$  for Figure 2c. Figure 2a shows the total transmittance over visible and near-infrared wavelengths with varying periods with  $w/\Lambda$  fixed at 0.5. Three cases are taken into consideration:  $\Lambda = 0.02$ , 0.4, and 2  $\mu$ m. It is observed that there is a larger discrepancy between transverse electric (TE) and transverse magnetic (TM) polarizations when the period is decreased. This discrepancy tends to be smaller and can be ignored with larger periods, as exemplified by the nearly overlapping TE and TM curves in Figure 2b with a period of 100  $\mu$ m. The total transmittance is the average of TE and TM values, and it depends on the filling ratio  $w/\Lambda$  rather than the period  $\Lambda$ . Therefore, a larger period  $\Lambda = 100 \ \mu m$  is chosen for the experiment, and it is easy for fabrication by photolithography.

The influence of Au layer thickness  $(h_3)$  is studied in Figure 2c. The transmittance is almost the same for gold thickness values of 50, 80, and 150 nm. Thinner values for the gold layer yield higher transmittance, as shown for the 20 nm case, indicating that transmittance is negatively correlated with Au





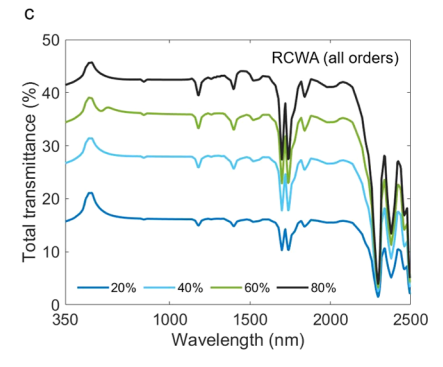
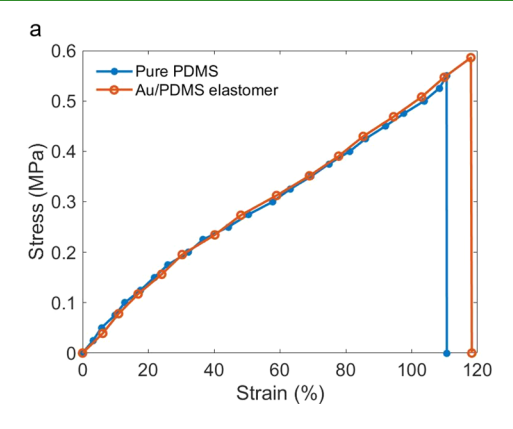


Figure 5. Experimental and calculated transmittance spectra for Scenario 1 structure from 350 to 2500 nm. (a) Experimental normal transmittances for strains varying from 0 to 80%. (b) Comparison between the experimental and calculated (RCWA) transmittances at three different strains: 20, 50, and 70%. (c) Calculated total transmittances for strains varying from 20 to 80%.



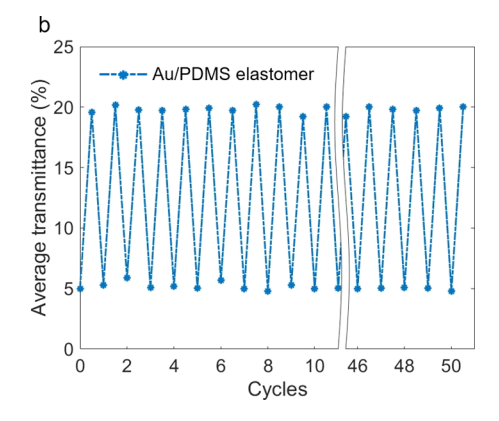


Figure 6. (a) Strain test for the pure PDMS grating sample and the Au-deposited elastomer. (b) Average transmittance of the Au-deposited elastomer through the cyclic stretching and releasing process.

layer thicknesses mainly between 20 and 50 nm. At thicknesses above 50 nm, Au can be regarded as a "bulk" material because its transmittance does not change greatly as a function of thickness above this value. Moreover, there exist maxima fixed at  $\lambda=500$  nm, corresponding to the natural color of the metal. The maxima of the transmission spectra are conditioned by the existence of bulk absorption modes according to their dispersion equation  $\omega=kc/\sqrt{\varepsilon(\omega)}$ , where k is the complex wavenumber, c is the light speed in vacuum, and  $\varepsilon(\omega)$  is the complex, frequency-dependent dielectric function. Therefore, the maximum occurs at  $\lambda=500$  nm in the transmittance spectra of Au films, offering an explanation for the natural yellowish color of Au.  $^{36}$ 

Next, Au/PDMS elastomers are fabricated to expand upon RCWA results. Figure 3 shows the fabrication process of the Au-deposited elastomer. A SU-8 mold is fabricated using photolithography. The base and curing agent of PDMS are mixed to a mass ratio of 10:1, degassed, and cured in a 60 °C oven. Au is deposited on the PDMS substrate using electron beam evaporation. More details on the fabrication process are provided in the Experimental Section. Scenarios 1 and 2 of Audeposited elastomers are fabricated to enable experimental testing with the following parameters:  $h_1 = 0.7$  mm,  $h_2 = 25$   $\mu$ m,  $h_3 = 75$  nm, w = 50  $\mu$ m, and  $\Lambda = 100$   $\mu$ m.

The stretching process is observed utilizing an optical microscope to clearly show how this Au-deposited elastomer behaves under applied stress. In Figure 4, the elastomers of both scenarios are stretched and then released to the original state. When no stress is applied to the elastomers, Au covers all

of the surfaces of the PDMS substrate for Scenario 1 (Figure 4a) and only the PDMS gratings for Scenario 2 (Figure 4b). After stretching the elastomers, for Scenario 1, two nonreflective areas of equal widths are observed between each Au stripe. As shown in the sketch of Figure 4a, these areas are due to the elongation of the PDMS substrate between the two layers of Au. The sketch represents an ideal case, where the thicknesses of the PDMS substrate, the PDMS grating, and the Au layer remain unchanged during the stretching. The widths of PDMS gratings and Au stripes are also considered as constant across the structure. For Scenario 2, it is shown that the widths of gratings and grooves elongate in the same proportion. Moreover, due to the Poisson's effect, compression along the transverse direction induces wrinkling in Au stripes, a phenomenon that is more apparent in Scenario 2. After releasing the tensile strain, wrinkling patterns become flattened, and the film surface reverts to the initial smooth state. This strain-tunable surface topography is used to regulate optical transmittance.

A spectrophotometer is then used to measure the normal transmittance (zeroth order) of the Au-deposited elastomer for Scenario 1 under different strains from 0 to 80% (Figure 5a). An increase in the normal transmittance through the visible and near-infrared wavelength regions is notable for increased amounts of strain. This is caused by the exposure of a more bare PDMS substrate when the elastomer is subjected to mechanical stress. An average transmittance tuning range from 5 to 20% is achieved by modulating between 0% strain and 80% strain. To verify the experimental results, the normal transmittance of this grating structure is calculated utilizing the

RCWA method, and the assumption of a constant Au width is made. In Figure 5b, at three different strains, the calculated and experimental results match quite well. Besides the perpendicular incidence, we also measure normal transmittances at incident angles of 0, 15, 30, and 45° when the Au/PDMS elastomer is in its original unstretched state (Figure S1a) as well as at a strain rate of 60% (Figure S1b). It is obviously shown that the normal transmittance is reduced with larger incident angles. This is because with oblique incident angles, the elongated PDMS between two layers of Au is blocked by the adjacent grating though non-Au-covered side walls are exposed to the light (Figure S1c). This transmittance tuning range can be further improved when considering the total transmittance, as scattering losses caused by the grating structure and the wrinkling pattern on Au stripes are present when evaluating the normal transmittance. Thus, there exists a discrepancy between the normal and total transmittance. As shown in Figure 5c, the total transmittance (all orders) calculated by the RCWA method is higher than the normal transmittance under the same strain in Figure 5a. The average total transmittance for 80% strain is 42%, double the average normal transmittance corresponding to the same strain.

In addition to a large transmittance modulation range, the maximum strain and durability are also key concerns for usage in practical applications. A strain test is carried out for the pure PDMS grating sample and the Au-deposited elastomer. From Figure 6a, it is seen that the two curves almost overlap, indicating that the mechanical properties of the two samples are similar. The pure PDMS and Au/PDMS elastomer fractures at 110 and 118% strains, respectively. The deposited nanometer-thickness Au has little influence on the Young's modulus of PDMS, which proves the feasibility of the mechanically induced transmittance modulator. A cyclic stretching and releasing experiment is conducted to verify the durability of the elastomer. One cycle consists of stretching the sample to 80% strain and then releasing the tensile force to return the sample to its original unstretched state. Figure 6b shows that over 50 cycles, the average transmittance is consistent when the elastomer is in the stretched state (20% transmittance) or original state (5% transmittance). Figure S2a,b shows the top-view SEM images of the sample before and after 50 cycles. After 50 cycles, the Au/PDMS interface still exhibits a good contact, and there is no obvious deposited Au peel-off, except that some wider cracks are generated due to the repeating stretching-releasing process. Thus, the Audeposited elastomer can be reversibly cycled without sacrificing structural integrity and optical performance.

This Au/PDMS elastomer provides a facile method to accomplish dynamic tuning of optical transmittance. In the previous work, reversible tuning by mechanical forces has been proposed, which harnesses surface wrinkles to scatter the incident light. While a large normal transmittance modulation is achieved, the total transmittance change is limited. In this work, both normal and total transmittance modulations have been realized through a stretchable Au/PDMS elastomer. When the elastomer works in its original state under solar irradiation, it blocks almost all of the incoming light. Upon stretching to 80% strain, the elastomer exhibits a large solar energy modulation of 42%, with a promising application in smart windows.

#### CONCLUSIONS

Switchable optical properties have garnered great attention in recent years due to their promising engineering applications, such as smart windows. Compared with chromogenic materials in response to external optical, thermal, electrical, and chemical stimuli, the tunable optical transmittance induced by mechanical force is the most straightforward and simple to accomplish. In this work, an elastomeric optical transmittance modulator is presented, composed of a stretchable PDMS substrate and employing Au as the reflective layer. The influences of geometric parameters on the total transmittance are evaluated by the RCWA method and show great agreement, indicating the applicability of this method for evaluating strain-based optical tuning. Microscopic images clearly show mechanisms by which the transmittance modulator deforms under a moderate strain and help to explain the optical behaviors that the modulator exhibits. The average normal transmittance is tuned from 5% at 0% strain to 20% at 80% strain, while the total transmittance can reach 42% at the same stretched state. The cycle test results promise both adequate structural integrity and consistent optical performance after repeated stretching and releasing processes. This mechanically induced elastomeric optical transmittance modulator is suitable for applications within many emerging optical systems that can leverage this technology. Furthermore, the simplistic tunable approach employed herein may be easily applied to other materials and geometries to further enhance tunability.

#### EXPERIMENTAL SECTION

**Mold Preparation.** The mold of the grating structure is built on a 4 inch diameter silicon wafer using photolithography. The wafer is cleaned using successive washes of acetone, methanol, and deionized water and dried on a hot plate. Photoresist SU-8 2025 is spin-coated onto the wafer using a Laurell Spinner. The thickness of the SU-8 layer is set at 25  $\mu$ m by choosing an appropriate spinning speed and time. Soft baking, exposure, and post exposure baking are performed according to basic photolithography procedures. The exposure time to ultraviolet light is 20 s, performed using Quintel 4000 mask aligner. The unexposed resist is dissolved by a SU-8 developer, while the exposed resist remains since SU-8 is a negative photoresist. Photolithography transfers the pattern from the mask to the photoresist layer.

**Sample Preparation.** PDMS samples are prepared using a commercially available kit (Sylgard 184, Dow Corning). The base and curing agent are mixed to a mass ratio of 10:1, degassed in a vacuum chamber for 30 min. The mass of the base and curing agent is calculated to achieve a PDMS substrate thickness of 0.7 mm. The mixture is then poured onto the SU-8 mold and cured in an oven at 60 °C for 150 min. The gold pellets (purity: 99.999%, 1/8" diameter  $\times$  1/8" long) are purchased from Kurt J. Lesker Company. Seventy-five nanometer Au is deposited on the PDMS substrate using the electron beam evaporation method at a vacuum of  $2 \times 10^{-6}$  Torr. The deposition rate is 3 Å s<sup>-1</sup>. For Scenario 2, the oblique angle deposition method is utilized. The sample is fixed on an adaptor, which changes the incident angle from the Au source. The incident angle depends on the geometric parameters of the PDMS grating.

**Material Characterizations.** The transmittance spectra in the range of 350–2500 nm are measured by the Jasco V770 spectrophotometer. The custom-built stretching device with a sample clamped on it is placed vertically to the optical path in the sample chamber. Without using the integrating sphere, only the normal transmittance is received by the detector. The background measurement is conducted when there is nothing inside the sample chamber. Different strains of the sample from 0 to 80% have been realized by this custom-built stretching device based on a high-precision

displacement-sliding table, and the corresponding normal transmittance data are recorded. For the cyclic test, the sample is stretched to 80% strain and then released to its original unstretched state. This stretching-releasing process is performed 50 times. Accessory for variable incident angle (VTA-752) is utilized for the measurement of oblique incidence. The morphology and structure of the Au-deposited elastomer are characterized by scanning electron microscopy (Supra 25 SEM). The microscope images are obtained using Metallurgical Microscope (AmScope, ME520TC-18M3) in the brightfield mode. The strain test is conducted using MARK-10 motorized test stands ESM303.

## ASSOCIATED CONTENT

## **Supporting Information**

The Supporting Information is available free of charge at https://pubs.acs.org/doi/10.1021/acsapm.1c00764.

Normal transmittances of the Au/PDMS elastomer with various incident angles and top-view SEM images before and after 50 cycles (PDF)

#### AUTHOR INFORMATION

## **Corresponding Author**

Yi Zheng — Department of Mechanical and Industrial Engineering, Northeastern University, Boston, Massachusetts 02115, United States; Department of Electrical and Computer Engineering, Northeastern University, Boston, Massachusetts 02115, United States; orcid.org/0000-0003-4963-9684; Email: y.zheng@northeastern.edu

#### **Authors**

Fangqi Chen – Department of Mechanical and Industrial Engineering, Northeastern University, Boston, Massachusetts 02115, United States

Yanpei Tian — Department of Mechanical and Industrial Engineering, Northeastern University, Boston, Massachusetts 02115, United States; oorcid.org/0000-0003-4181-9517

Xiaojie Liu — Department of Mechanical and Industrial Engineering, Northeastern University, Boston, Massachusetts 02115, United States

Andrew Caratenuto — Department of Mechanical and Industrial Engineering, Northeastern University, Boston, Massachusetts 02115, United States

Complete contact information is available at: https://pubs.acs.org/10.1021/acsapm.1c00764

#### Notes

The authors declare no competing financial interest.

## ■ ACKNOWLEDGMENTS

This project is supported by the National Science Foundation through grant no. CBET-1941743.

## **■** REFERENCES

- (1) Ge, D.; Lee, E.; Yang, L.; Cho, Y.; Li, M.; Gianola, D. S.; Yang, S. A robust smart window: reversibly switching from high transparency to angle-independent structural color display. *Adv. Mater.* **2015**, *27*, 2489–2495.
- (2) Baetens, R.; Jelle, B. P.; Gustavsen, A. Properties, requirements and possibilities of smart windows for dynamic daylight and solar energy control in buildings: A state-of-the-art review. *Sol. Energy Mater. Sol. Cells* **2010**, *94*, 87–105.
- (3) Cupelli, D.; Nicoletta, F. P.; Manfredi, S.; Vivacqua, M.; Formoso, P.; de Filpo, G.; Chidichimo, G. Self-adjusting smart

- windows based on polymer-dispersed liquid crystals. Sol. Energy Mater. Sol. Cells 2009, 93, 2008–2012.
- (4) Granqvist, C. G. Electrochromic tungsten oxide films: review of progress 1993-1998. Sol. Energy Mater. Sol. Cells 2000, 60, 201–262.
- (5) Granqvist, C. G. Electrochromics for smart windows: Oxide-based thin films and devices. *Thin Solid Films* **2014**, *564*, 1–38.
- (6) Mu, J.; Hou, C.; Wang, G.; Wang, X.; Zhang, Q.; Li, Y.; Wang, H.; Zhu, M. An elastic transparent conductor based on hierarchically wrinkled reduced graphene oxide for artificial muscles and sensors. *Adv. Mater.* **2016**, 28, 9491–9497.
- (7) Zeng, S.; Li, R.; Freire, S. G.; Garbellotto, V. M.; Huang, E. Y.; Smith, A. T.; Hu, C.; Tait, W. R.; Bian, Z.; Zheng, G.; Zhang, D.; Sun, L. Moisture-responsive wrinkling surfaces with tunable dynamics. *Adv. Mater.* **2017**, 29, No. 1700828.
- (8) Wang, W.; Ye, Y.; Feng, J.; Chi, M.; Guo, J.; Yin, Y. Enhanced Photoreversible Color Switching of Redox Dyes Catalyzed by Barium-Doped TiO2 Nanocrystals. *Angew. Chem., Int. Ed.* **2015**, *54*, 1321–1326.
- (9) Vergaz, R.; Sanchez-Pena, J.-M.; Barrios, D.; Vazquez, C.; Contreras-Lallana, P. Modelling and electro-optical testing of suspended particle devices. *Sol. Energy Mater. Sol. Cells* **2008**, 92, 1483–1487.
- (10) Sheraw, C.; Zhou, L.; Huang, J.; Gundlach, D.; Jackson, T.; Kane, M.; Hill, I.; Hammond, M.; Campi, J.; Greening, B.; Francl, J.; West, J. Organic thin-film transistor-driven polymer-dispersed liquid crystal displays on flexible polymeric substrates. *Appl. Phys. Lett.* **2002**, *80*, 1088–1090.
- (11) Wang, W.; Feng, J.; Ye, Y.; Lyu, F.; Liu, Y.-s.; Guo, J.; Yin, Y. Photocatalytic color switching of transition metal hexacyanometalate nanoparticles for high-performance light-printable rewritable paper. *Nano Lett.* **2017**, *17*, 755–761.
- (12) Han, D.; Jiang, B.; Feng, J.; Yin, Y.; Wang, W. Photocatalytic Self-Doped SnO2- x Nanocrystals Drive Visible-Light-Responsive Color Switching. *Angew. Chem., Int. Ed.* **2017**, *56*, 7792–7796.
- (13) Parkin, I. P.; Manning, T. D. Intelligent thermochromic windows. J. Chem. Educ. 2006, 83, No. 393.
- (14) Dyer, A. L.; Grenier, C. R.; Reynolds, J. R. A Poly (3, 4-alkylenedioxythiophene) Electrochromic Variable Optical Attenuator with Near-Infrared Reflectivity Tuned Independently of the Visible Region. *Adv. Funct. Mater.* **2007**, *17*, 1480–1486.
- (15) Bechinger, C.; Ferrere, S.; Zaban, A.; Sprague, J.; Gregg, B. A. Photoelectrochromic windows and displays. *Nature* **1996**, 383, 608–610.
- (16) Hoi, S.-K.; Chen, X.; Kumar, V. S.; Homhuan, S.; Sow, C.-H.; Bettiol, A. A. A microfluidic chip with integrated colloidal crystal for online optical analysis. *Adv. Funct. Mater.* **2011**, *21*, 2847–2853.
- (17) Li, Z.; Zhai, Y.; Wang, Y.; Wendland, G. M.; Yin, X.; Xiao, J. Harnessing surface wrinkling-cracking patterns for tunable optical transmittance. *Adv. Opt. Mater.* **2017**, *5*, No. 1700425.
- (18) Zeng, S.; Zhang, D.; Huang, W.; Wang, Z.; Freire, S. G.; Yu, X.; Smith, A. T.; Huang, E. Y.; Nguon, H.; Sun, L. Bio-inspired sensitive and reversible mechanochromisms via strain-dependent cracks and folds. *Nat. Commun.* **2016**, *7*, No. 11802.
- (19) Ciardelli, F.; Ruggeri, G.; Pucci, A. Dye-containing polymers: methods for preparation of mechanochromic materials. *Chem. Soc. Rev.* **2013**, *42*, 857–870.
- (20) Martínez, L. M. T.; Kharissova, O. V.; Kharisov, B. I. Handbook of Ecomaterials; Springer, 2019.
- (21) Yang, D.; Kong, X.; Ni, Y.; Ren, Z.; Li, S.; Nie, J.; Chen, X.; Zhang, L. Ionic polymer-metal composites actuator driven by the pulse current signal of triboelectric nanogenerator. *Nano Energy* **2019**, 66, No. 104139.
- (22) Li, S.; Nie, J.; Shi, Y.; Tao, X.; Wang, F.; Tian, J.; Lin, S.; Chen, X.; Wang, Z. L. Contributions of different functional groups to contact electrification of polymers. *Adv. Mater.* **2020**, 32, No. 2001307.
- (23) Li, S.; Fan, Y.; Chen, H.; Nie, J.; Liang, Y.; Tao, X.; Zhang, J.; Chen, X.; Fu, E.; Wang, Z. L. Manipulating the triboelectric surface

- charge density of polymers by low-energy helium ion irradiation/implantation. *Energy Environ. Sci.* **2020**, *13*, 896–907.
- (24) Meng, Q.; Cai, K.; Chen, Y.; Chen, L. Research progress on conducting polymer based supercapacitor electrode materials. *Nano Energy* **2017**, *36*, 268–285.
- (25) Wang, Y.; Chen, F.; Liu, Z.; Tang, Z.; Yang, Q.; Zhao, Y.; Du, S.; Chen, Q.; Zhi, C. A highly elastic and reversibly stretchable all-polymer supercapacitor. *Angew. Chem.* **2019**, *131*, 15854–15858.
- (26) Lee, K. Y.; Kumar, B.; Seo, J.-S.; Kim, K.-H.; Sohn, J. I.; Cha, S. N.; Choi, D.; Wang, Z. L.; Kim, S.-W. P-type polymer-hybridized high-performance piezoelectric nanogenerators. *Nano Lett.* **2012**, *12*, 1959–1964.
- (27) Jung, I.; Shin, Y.-H.; Kim, S.; Choi, J.-y.; Kang, C.-Y. Flexible piezoelectric polymer-based energy harvesting system for roadway applications. *Appl. Energy* **2017**, 197, 222–229.
- (28) Park, D.; Kim, P.; Alvarenga, J.; Jin, K.; Aizenberg, J.; Bechthold, M. Dynamic daylight control system implementing thin cast arrays of polydimethylsiloxane-based millimeter-scale transparent louvers. *Build. Environ.* **2014**, *82*, 87–96.
- (29) Lee, S. G.; Lee, D. Y.; Lim, H. S.; Lee, D. H.; Lee, S.; Cho, K. Switchable transparency and wetting of elastomeric smart windows. *Adv. Mater.* **2010**, 22, 5013–5017.
- (30) Lee, E.; Zhang, M.; Cho, Y.; Cui, Y.; van der Spiegel, J.; Engheta, N.; Yang, S. Tilted pillars on wrinkled elastomers as a reversibly tunable optical window. *Adv. Mater.* **2014**, *26*, 4127–4133.
- (31) Zhu, Y.; Antao, D. S.; Xiao, R.; Wang, E. N. Real-Time Manipulation with Magnetically Tunable Structures. *Adv. Mater.* **2014**, *26*, 6442–6446.
- (32) Cao, C.; Chan, H. F.; Zang, J.; Leong, K. W.; Zhao, X. Harnessing localized ridges for high-aspect-ratio hierarchical patterns with dynamic tunability and multifunctionality. *Adv. Mater.* **2014**, *26*, 1763–1770.
- (33) Zang, J.; Ryu, S.; Pugno, N.; Wang, Q.; Tu, Q.; Buehler, M. J.; Zhao, X. Multifunctionality and control of the crumpling and unfolding of large-area graphene. *Nat. Mater.* **2013**, *12*, 321–325.
- (34) Thomas, A. V.; Andow, B. C.; Suresh, S.; Eksik, O.; Yin, J.; Dyson, A. H.; Koratkar, N. Controlled crumpling of graphene oxide films for tunable optical transmittance. *Adv. Mater.* **2015**, *27*, 3256–3265
- (35) Jiang, B.; Liu, L.; Gao, Z.; Wang, W. A general and robust strategy for fabricating mechanoresponsive surface wrinkles with dynamic switchable transmittance. *Adv. Opt. Mater.* **2018**, *6*, No. 1800195.
- (36) Axelevitch, A.; Apter, B.; Golan, G. Simulation and experimental investigation of optical transparency in gold island films. *Opt. Express* **2013**, *21*, 4126–4138.